nanomaterials

MDPI

Article

Enhanced Photoluminescence of $Gd_3Al_4GaO_{12}$: Cr^{3+} by Energy Transfers from Co-Doped Dy^{3+}

Yu Zhang [1,2,†], Xiang Li [1,2,†], Dahai Hu [1,2], Qier Sa [1,2], Xinran Wang [1,2], Fengxiang Wang [1,2], Kaixuan Wang [1,2], Xuelian Zhou [1,2], Zhiqiang Song [1,2], Yongfu Liu [3] and Kefu Chao [1,2,*]

1 Inner Mongolia Key Laboratory of Physics and Chemistry of Functional Materials, College of Physics and Electronic Information, Inner Mongolia Normal University, Hohhot City 010022, China
2 Inner Mongolia Engineering Research Center for Rare Earth Functional and New Energy Storage Materials, Hohhot City 010022, China
3 Ningbo Institute of Materials Technology and Engineering, Chinese Academy of Sciences, Ningbo 315201, China
* Correspondence: phyerick@imnu.edu.cn; Tel.: +86-4717383862
† These authors contributed equally to this work.

Abstract: LEDs for plant lighting have attracted wide attention and phosphors with good stability and deep-red emission are urgently needed. Novel Cr^{3+} and Dy^{3+} co-doped $Gd_3Al_4GaO_{12}$ garnet (GAGG) phosphors were successfully prepared through a conventional solid-state reaction. Using blue LEDs, a broadband deep-red emission at 650–850 nm was obtained due to the Cr^{3+} $^4T_2 \rightarrow {}^4A_2$ transition. When the Cr^{3+} concentration was fixed to 0.1 mol, the crystal structure did not change with an increase in the Dy^{3+} doping concentration. The luminous intensity of the optimized GAGG:0.1Cr^{3+}, 0.01Dy^{3+} was 1.4 times that of the single-doped GAGG:0.1Cr^{3+}. Due to the energy transfer from Dy^{3+} to Cr^{3+}, the internal quantum efficiency reached 86.7%. The energy transfer from Dy^{3+} to Cr^{3+} can be demonstrated through luminescence spectra and fluorescence decay. The excellent properties of the synthesized phosphor indicate promising applications in the agricultural industry.

Keywords: $Gd_3Al_4GaO_{12}$:Cr^{3+}, Dy^{3+}; phosphors; energy transfer; LEDs

Citation: Zhang, Y.; Li, X.; Hu, D.; Sa, Q.; Wang, X.; Wang, F.; Wang, K.; Zhou, X.; Song, Z.; Liu, Y.; et al. Enhanced Photoluminescence of $Gd_3Al_4GaO_{12}$: Cr^{3+} by Energy Transfers from Co-Doped Dy^{3+}. *Nanomaterials* **2022**, *12*, 4183. https://doi.org/10.3390/nano12234183

Academic Editors: David F. Kelley and Antonino Gulino

Received: 31 October 2022
Accepted: 22 November 2022
Published: 25 November 2022

1. Introduction

Lighting is one important factors affecting plant growth. Photopigment P_R and P_{FR} mainly absorb deep-red light at 660–730 nm. P_R and P_{FR} play vital roles at all stages of plant growth and development, such as promoting seed germination, desiccating, stem growth, leaf expansion, shading and inducing effects, etc. [1–4]. However, traditional light sources, such as incandescent lamps, metal halide lamps, fluorescent lamps, and high-pressure sodium lamps, have the disadvantages of high costs and short lives. At present, the white LEDs existing in the market mainly cover the yellow-green wavelength range [5,6], and the near-infrared LEDs do not match well with the chlorophyll absorption band of plants because of their narrow luminous wavelength and low luminous intensity [7–9]. Therefore, broad, deep-red lighting devices suitable for plant growth have become the focus [10]. At present, phosphor-converted light-emitting diodes (pcLEDs) based on blue chips, are among the most effective lighting means [11–14].

They are energy efficient, ensure environmental protection, and a have long service life, a small size, and low costs. Red emission phosphors, such as (Sr, Ca)$AlSiN_3$:Eu^{2+} [15], and K_2TiF_6:Mn^{4+} [16], have become commercially available to improve the color quality of white LEDs. However, their emission wavelengths cannot be tuned to the deep-red band and the strongest emission cannot be effectively absorbed by plants. In addition, the nitride synthesis conditions are harsh, rare-earth materials are expensive, and the mining/purification process of Eu^{2+} is harmful to the environment, making it expensive and less stable [17]. Further K_2TiF_6:Mn^{4+} phosphor cannot provide an effective absorption

band of red light covered plants with broad spectra. Thus, how to achieve broad, deep-red phosphors that can be efficiently excited by blue light is a more important challenge [7].

Recently, materials doped with the transition-metal ion Cr^{3+} have been considered to be ideal red phosphors. Its 3d electrons are located in the outer layer and are very sensitive to the crystal environment [18–22]. Therefore, the selection of different matrices allows for tunable emission for Cr^{3+} from deep-red to NIR light by adjusting the surrounding crystal field environment. The $Gd_3Al_4GaO_{12}$ garnet (GAGG) is a stable material for scintillators and phosphors that have a lower synthesis temperature compared to the commonly used garnets [23]. Karolina Elzbieciak and Lukasz Marciniak reported the strategy for modulating the relative sensitivity of Cr^{3+}-based luminescent thermometers through substituting Al^{3+} ions with Ga^{3+} in $Gd_3Al_{5-x}Ga_xO_{12}:Cr^{3+}$, Nd^{3+} and caused the gradual decline of the crystal field strength from Dq/B = 2.69 to Dq/B = 2.18, respectively, for $Gd_3Al_5O_{12}:Cr^{3+}$, Nd^{3+} and $Gd_3Ga_5O_{12}:Cr^{3+}$, Nd^{3+} [24]. Zhang et al. reported on broad-band near-infrared $Ca_2LuZr_2Al_3O_{12}:Cr^{3+}$ garnet phosphor, which was used in combination with a 460 nm LED chip to fabricate pc-LED devices. Its photoelectric efficiency was 4.1%, which was better than that of tungsten lamps (2.9%) in the 750–820 nm spectrum range [25]. Cr^{3+} had the advantage of high efficiency and matching with blue LED chips compared to other NIR phosphors. However, the luminous efficiency needs further improvement.

Cr^{3+} luminescence can suffer from impurities and oxidation into Cr^{4+} when the materials are sintered in the air. As a result, the luminous efficiency of Cr^{3+} doped substrates reported so far has not been very high because of impurities. For instance, the external quantum efficiency (EQE) of $Ca_3Sc_2Si_3O_{12}$ (CSSG) was 12.8% [26]. The external quantum efficiency was increased to 21.5% by adding flux and sintering in a CO-reducing atmosphere [7]. In addition, rare-earth/Cr^{3+} co-doping appears to be a very promising method of improving luminous efficiency. For instance, a $Ca_2LuHf_2Al_3O_{12}:Ce^{3+}$, Cr^{3+} sample synthesized using a conventional high-temperature solid-phase method is three times brighter than a single-doped Cr^{3+}. Therefore, rare-earth/Cr^{3+} co-doping appears to be a very promising method of improving luminous efficiency [27].

In this paper, GAGG:Cr^{3+}, Dy^{3+} samples were synthesized using a conventional high-temperature solid-phase method to obtain phosphors with high brightness and deep-red luminescence. The synthesis method is environment-friendly, simple, and cheap and leads to a pure $Gd_3Al_4GaO_{12}$ phase. In GAGG:Cr^{3+}, the absorption of Cr^{3+} comes from the d-d forbidden transition, its excitation efficiency is low. In order to obtain higher luminescence intensity, the sensitized ion Dy^{3+} was introduced into the GAGG:Cr^{3+} material. The energy transfer process between Cr^{3+} and Dy^{3+} in the GAGG is addressed. To the best of our knowledge, this is the first report detailing an energy transfer and the luminescent properties of a Cr^{3+}-Dy^{3+} co-doped GAGG host. Moreover, this work represents an advance in the development and application of plant growth lighting.

2. Experimental Section

A conventional high-temperature solid-phase method was used to synthesize GAGG:Cr^{3+}, Dy^{3+} samples. The stoichiometries were $Gd_{3-y}Al_{4-x}GaO_{12}:xCr^{3+}$, yDy^{3+} with x = 0, 0.08, 0.1, 0.15, 0.2 and y = 0, 0.002, 0.006, 0.01, 0.014, 0.018. Gd_2O_3 (Aladdin, 99.99%) (Shanghai, China), Al_2O_3 (Aladdin, 99.9%), Ga_2O_3 (Aladdin, 99.99%), Cr_2O_3 (Aladdin, 99.99%), and Dy_2O_3 (Aladdin, 99.99%) were used as starting materials, and 0.07 mol of H_3BO_3 (Aladdin, 99.9%) was added as the flux. The above materials were weighed according to the stoichiometric ratio, grounded evenly in an agate mortar, mixed into corundum crucibles, and annealed at 1650 °C for 6 h in a box-type resistance furnace using a rate of 10 °C/min. The samples were protected by 5% H_2/N_2 gas flow during the whole sintering process. The calcined sample is naturally cooled to room temperature and grounded evenly to obtain a series of phosphor powders.

Powder X-ray diffraction was measured at room temperature using a PANalytical heaven II diffractometer employing CuKα radiation. The scanning step was 0.02° in the range of 10–90° with 4 s per step integration. A scanning electron microscope (SEM,

Hitachi S-3400-N, Homewood, AL, USA) was used to observe the product morphology. A fluorescence spectrophotometer (FS5, Edinburgh, Livingston, UK) equipped with a 450 W xenon lamp, was used to record the excitation and emission spectra of the samples and explore their luminescence performances. The thermal quenching test was completed using the FLS980 steady state transient fluorescence/phosphorescence spectrometer. The corresponding temperature-dependent emission properties of as-synthesized phosphors were measured on the FS5 fluorescence spectrometer. The temperature of the samples was controlled through an externally connected temperature controller (Orient KOJI, Hongkong, China). The samples were heated from 25 to 200 °C at a constant rate of 5 °C/min. The (EVERFINE) analysis system was used to test the packaged sample device.

3. Results and Discussion

3.1. Phase Identification and Crystal Structure

The XRD patterns of GAGG, GAGG:0.1Cr^{3+}, and GAGG:0.1Cr^{3+}, 0.01Dy^{3+} are shown in Figure 1a. These samples were basically consistent with the standard card (PDF # 46-0447). After Dy^{3+} doping, the XRD patterns shown in Figure 1b shifted toward smaller angles, which proved the successful doping of Dy^{3+}. The shift was less pronounced after co-doping with Cr^{3+}, indicating that the single Cr^{3+} doping or Cr^{3+} and Dy^{3+} co-doping had little effect on the matrix lattice parameters. The ionic radius of Cr^{3+} was 0.615 Å (CN = 6), Al^{3+} was 0.540 Å (CN = 6), Dy^{3+} was 0.912 Å (CN = 8) and Gd^{3+} was 0.938 Å (CN = 8); therefore, it is most likely that Dy^{3+} fits in the Gd^{3+} sites. Cr^{3+} is expected to emit near-infrared light in an octahedral rather than a tetrahedral environment, so Cr^{3+} prefers to replace Al^{3+} in an octahedral environment rather than Ga^{3+} in a tetrahedral environment [28–30]. All diffraction peaks were well indexed to GAGG, as shown in Figure 1a,c, and calculated using the Rietveld structure refinement method. Additionally, no extra peak appeared in the patterns, indicating that pure phase GAGG:Cr^{3+}, Dy^{3+} phosphors had been achieved. Figure 1d shows the dodecahedral, octahedral, and tetrahedral positions. In the GAGG structure, the dodecahedral lattice (24c lattice) was occupied by Gd^{3+}, and Al^{3+} and Ga^{3+} occupied octahedral and tetrahedral positions. However, when Cr^{3+} ions were doped into the system, they gave preference to octahedral coordination and then entered the tetrahedra.

Figure 2a,b presents SEM images of GAGG:0.1Cr^{3+} and GAGG:0.1Cr^{3+}, 0.01Dy^{3+}. EDX scanning was performed at 15 keV and 10 k magnification. Since the samples were ground, they showed an almost identical irregular morphology. Figure 2c,d shows the EDS energy spectra of GAGG: 0.1Cr^{3+} and GAGG:0.1Cr^{3+},0.01Dy^{3+}. The EDS analysis confirmed that the samples contained Gd^{3+}, Ga^{3+}, O^{2-}, Al^{3+}, Cr^{3+} and Dy^{3+} as trace elements. XRD and SEM/EDS results, therefore, confirmed that Cr^{3+} and Dy^{3+} ions were successfully doped into the GAGG matrix.

3.2. Luminescence Properties

The excitation and emission spectra of GAGG:Cr^{3+} are shown in Figure 3a. There are two excitation bands at 350–500 nm and 500–650 nm, which belong to the $^4A_2 \rightarrow {}^4T_1$ and the $^4A_2 \rightarrow {}^4T_2$ transitions of Cr^{3+}, respectively. Under the 450 nm excitation, the characteristic Cr^{3+} emission composed of narrow peaks at 693 and 713 nm in the range of 650–850 nm, was observed. The emission from 650 to 850 nm originates from the $^4T_2 \rightarrow {}^4A_2$ transition. The peak at 693 nm originates from the zero phonon line of the $^2E \rightarrow {}^4A_2$ spin forbidden transition (the R line) [31–33].

Typically, the Cr^{3+} sample shows a sharp line normally attributed to the spin-forbidden leap $^2E \rightarrow {}^4A_2$ [29]. The excitation spectra of GAGG:Cr^{3+} were mainly located in the blue light region, indicating that the GAGG:Cr^{3+} phosphor matches well with the emission of blue LED chips. The emission of GAGG:Cr^{3+} is located in the deep-red region and has a good overlap with the absorption spectrum of photosensitive pigments P_R and P_{FR}. LEDs constructed using the GAGG:Cr^{3+} phosphor and blue chips could be ideal lighting devices for plant lighting.

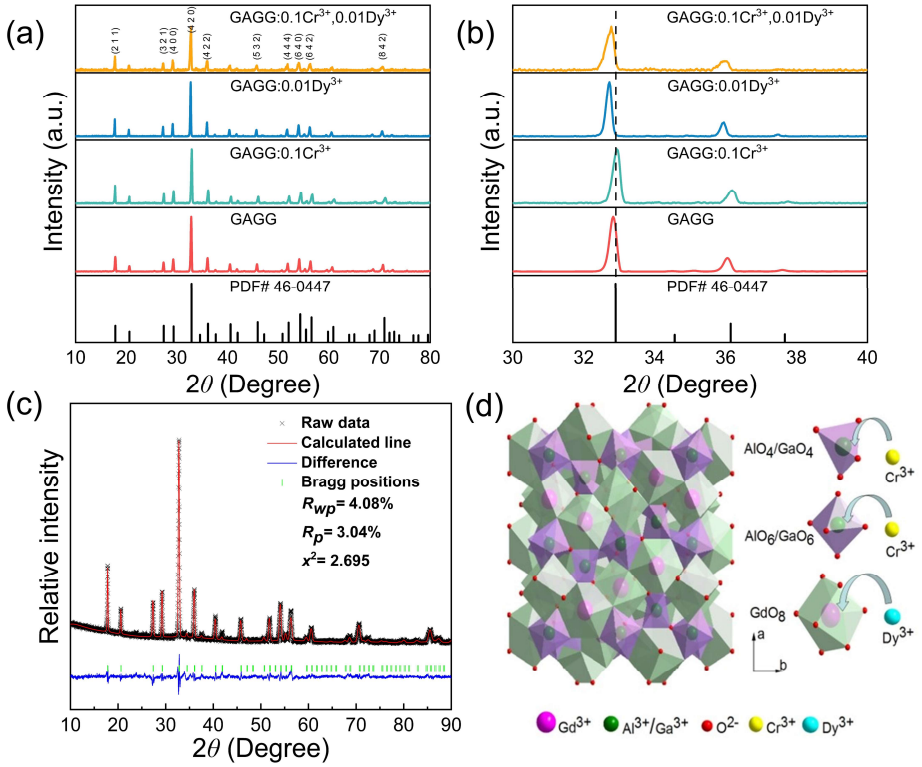

Figure 1. (**a**) XRD of GAGG, GAGG:Cr^{3+}, GAGG:Dy^{3+} and GAGG:Cr^{3+}, Dy^{3+}; (**b**) magnified XRD patterns in the 30–40° range; (**c**) XRD refinements of GAGG; (**d**) crystal structure of GAGG viewed along the a-axis.

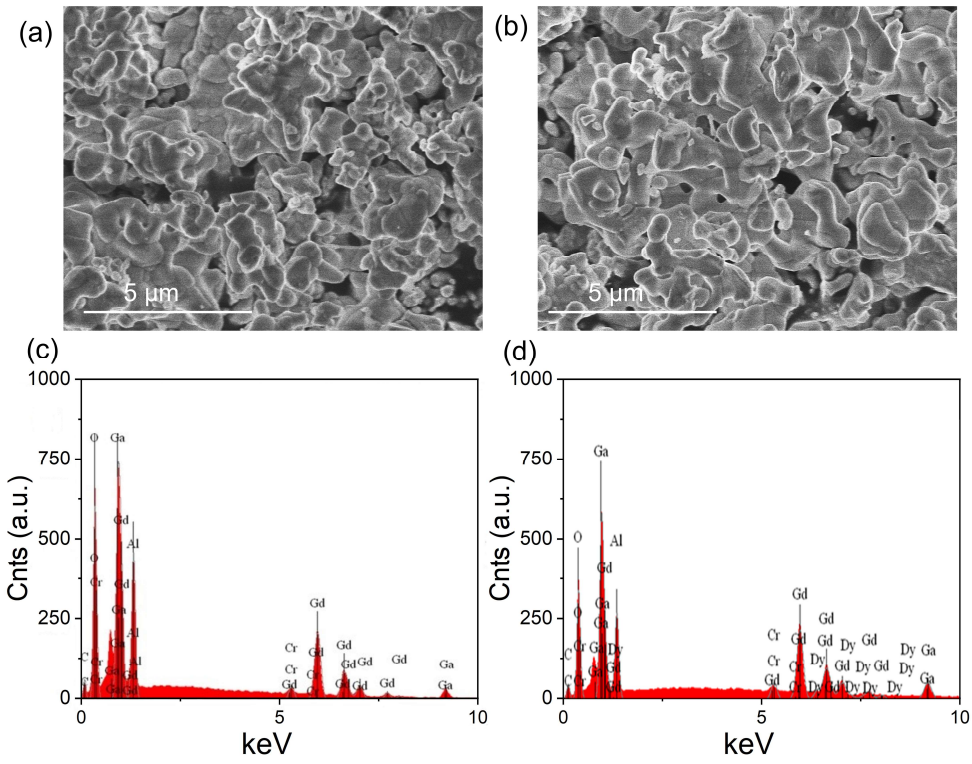

Figure 2. SEM photographs of GAGG:Cr^{3+} (**a**) and GAGG:0.1Cr^{3+}, 0.01Dy^{3+} (**b**). EDS of GAGG:0.1Cr^{3+} (**c**) and GAGG:0.1Cr^{3+}, 0.01Dy^{3+} (**d**).

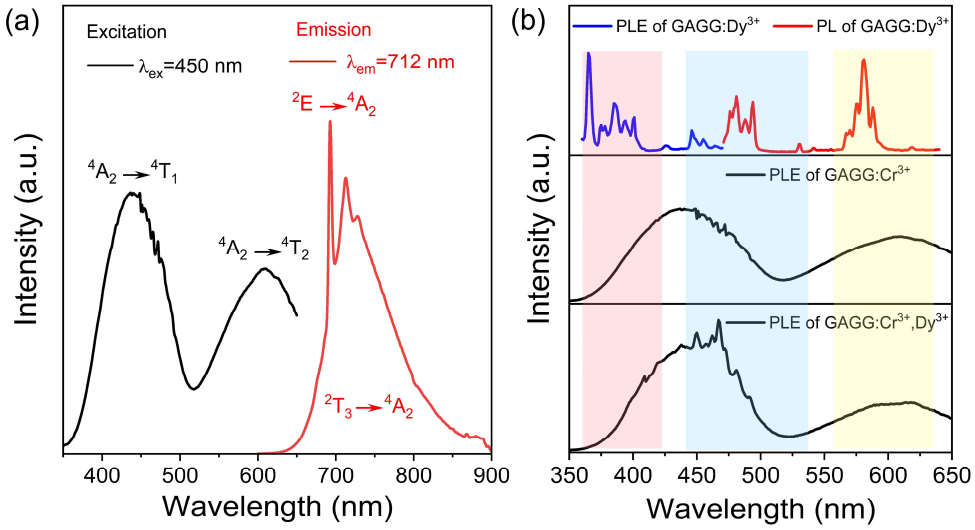

Figure 3. (**a**) PLE (λem = 712 nm) and PL (λex = 450 nm) spectra of GAGG:0.1Cr^{3+}; (**b**) PL spectrum of GAGG:Cr^{3+} and GAGG:Cr^{3+}, Dy^{3+} (black line), the PL (Blue line) and PLE spectra (red line) of GAGG:Dy^{3+}.

The PLE (blue line) and PL (red line) spectra of GAGG:0.01Dy^{3+} are shown in Figure 3b. A wavelength of 575 nm was selected to detect the PLE spectrum, and a 450 nm wavelength was used to excite the sample. The excitation peaks at 352, 366, 387, 427, 452, and 476 nm were attributed to the Dy^{3+} transition from $^6H_{15/2}$ to $^6p_{7/2}$, $^6p_{5/2}$, $^4p_{7/2}$, $^4G_{11/2}$, $^4I_{15/2}$, and $^4F_{9/2}$, respectively [34,35]. The emission peaks at 479 and 575 nm were attributed to the $^4F_{9/2} \rightarrow {}^6H_{15/2}$ and $^4F_{9/2} \rightarrow {}^6H_{13/2}$ transitions, respectively [36,37]. The PLE spectra show that both Cr^{3+} and Dy^{3+} can be excited by blue light at 450 nm. It is also found that the emission peak of Dy^{3+} overlapped with the excitation peak of Cr^{3+}; thus, energy transfers in the Cr^{3+}-Dy^{3+} co-doped sample were possible.

The luminescence properties of Cr^{3+} and Dy^{3+} co-doped GAGG were further investigated, as shown in Figure 4. The content of Cr^{3+} was fixed at 0.1 mol, and the Dy^{3+} ion doping concentration changed from 0.002 to 0.18. For GAGG:0.1 Cr^{3+},0.01Dy^{3+}, the luminescence intensity was the highest and the luminescence intensity was 1.4 times that of the Cr^{3+} single doped sample. At the same time, the internal quantum efficiency of GAGG:0.1 Cr^{3+},0.01Dy^{3+} reached the maximum of 86.65%. Even more interestingly, only the emission of Cr^{3+} was produced in GAGG:Cr^{3+},0.01Dy^{3+}. Concentration quenching started to occur when the concentration of Dy^{3+} was greater than 0.01. This was probably caused by a total energy transfer from $^4F_{7/2}$ toward $^4T_2$ levels and to the E_g level that led to deep-red emission [25]. There was an energy transfer between Dy^{3+} and Cr^{3+}. In addition, it was found that the addition of Dy^{3+} did not affect the luminescence peak position and waveform of Cr^{3+}. Since the radius of Dy^{3+} (0.912 Å, CN = 8) was almost equal to that of Gd^{3+} (0.938 Å CN = 8), Dy^{3+} entered the lattice and only occupied the position of Gd^{3+}, and the formed REO_8 (RE = Gd, Dy) hardly affected the crystal field of the neighboring of CrO_6 (GaO_6) octahedrons [38].

3.3. Energy Transfer in GAGG: Cr^{3+}, Dy^{3+}

In order to further study the energy transfer between Dy^{3+} and Cr^{3+}, the fluorescent decays of Dy^{3+} were measured, as shown in Figure 5a. The fluorescence attenuation curves of GAGG: $x$$Cr^{3+}$, 0.01$Dy^{3+}$ (x = 0, 0.08, 0.1, 0.15, 0.2) were measured under the 450 nm excitation and the 575 nm detection. The fluorescence attenuation curve was fitted using a second-order exponential attenuation model, with the formula as follows [39].

$$I = I_0 + A_1 \exp(-t/\tau_1) + A_2 \exp(-t/\tau_2) \quad (1)$$

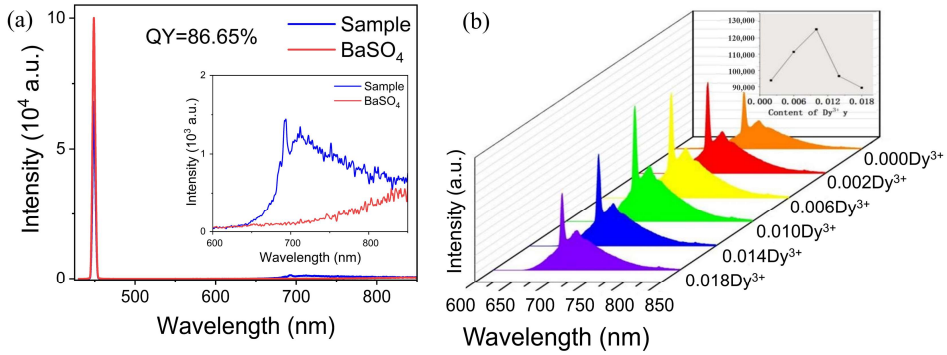

Figure 4. (**a**) Normalized spectra of the 450 nm light with $BaSO_4$ as reference for quantum efficiency measurement and of GAGG:0.1Cr^{3+},0.01Dy^{3+}; (**b**) emission spectra (λ_{ex} = 450 nm) of GAGG:0.1Cr^{3+}, $y$$Dy^{3+}$ (y = 0, 0.002, 0.006, 0.01, 0.014, 0.018).

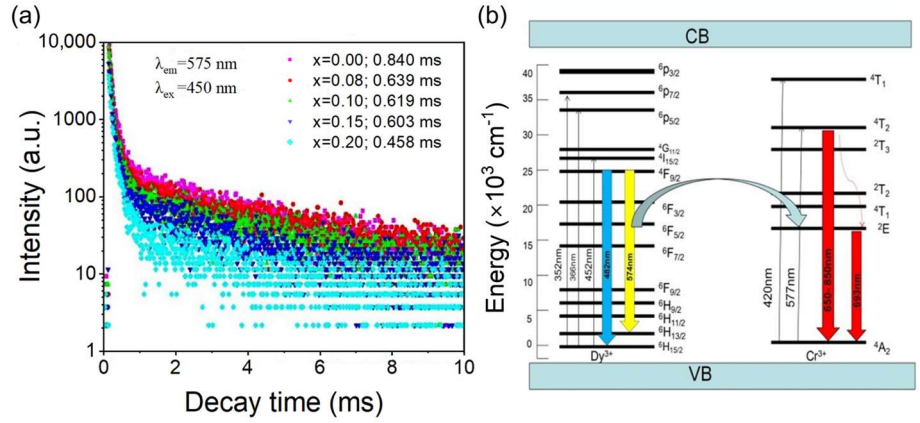

Figure 5. (**a**) Decay curves of Dy^{3+} emission in GAGG:$x$$Cr^{3+}$, 0.01$Dy^{3+}$; (**b**) energy levels, electron transitions and energy transfer schematic diagram of Dy^{3+} and Cr^{3+} in GAGG.

A_1 and A_2 are the fitting constants, I is the intensity of fluorescence at time t, τ_1 and τ_2 are the fluorescence lifetime; The average attenuation-times are also fitted with a second-order index, as shown in Formula (2) [40].

$$\tau = \left(A_1\tau_1^2 + A_2\tau_2^2\right)/(A_1\tau_1 + A_2\tau_2) \quad (2)$$

The fluorescence lifetime decreased from 0.84 to 0.458 ms with increasing Cr^{3+} concentration from 0 to 0.2 respectively. This result proves that energy transfers from Dy^{3+} to Cr^{3+} existed in these samples. We note a somewhat similar phenomenon in the $Ca_{14}(Al, Ga)_{10}Zn_6O_{35}$ matrix to what was reported by Zhou et al. [41].

The following equation can be used to calculate the energy transfer efficiency (η_{ET}) [42].

$$\eta_{ET} = 1 - \tau_s/\tau_{s0} \quad (3)$$

where τ and τ_0 are the lifetimes of Dy^{3+} with and without Cr^{3+}. On the basis of the formula, the energy transfer efficiency increased from 23.9% to 45.48%.

To describe the energy change in GAGG:0.1Cr^{3+},0.01Dy^{3+} phosphor, the excitation, emission and energy transfer processes are shown in Figure 5b. Under the irradiation of 450 nm light, electrons are excited from the Dy^{3+} $^6H_{15/2}$ energy level to the excited state, such as $^6p_{7/2}$, $^6p_{5/2}$, $^4p_{7/2}$, $^4G_{11/2}$, $^4I_{15/2}$, and $^4F_{9/2}$, and then relax to $^6H_{13/2}$ and $^6H_{15/2}$ from $^4F_{9/2}$ with blue and orange emission. Meanwhile, electrons can also be excited into the Cr^{3+} $^4T_1$ and then relax to the $^4T_2$ and ^2E energy levels, thus providing deep-red emission when relaxing to the $^4A_2$ state. In this process, the energy transfer occurs from the excited state $^4F_{9/2}$ of Dy^{3+} to the excited states $^4T_2$ and ^2E of Cr^{3+}.

3.4. Temperature-Dependent Emission Spectra

The normalized emission intensity, as a function of temperature is shown in Figure 6a. When the temperature is 440 K, the light intensities at 693 and 712 nm are 73.4% and 81.6%, respectively, of those at 300 K. Figure 6b illustrates the emission spectra of GAGG:0.1Cr^{3+}, 0.01Dy^{3+} excited at 450 nm in the temperature range of 300–470 K. The profiles of the PL spectra do not experience major changes at different temperatures, while the intensity decreases with increasing temperatures owing to the thermal quenching effect [32]. Figure 6c shows the projection of the emission spectrum with increasing temperature, which shows the change of luminous intensity with increasing temperature. The increase in temperature leads to the intensification of lattice vibrations and an increase in the probability of non-radiative relaxations. The particles of each metastable state relax back to the ground state without radiation, and finally, the excitation energy is dissipated in the matrix lattice in the form of thermal energy. Compared with the spin-allowed transition from $^4T_2$ (4F) to $^4A_2$, the lattice vibration has a greater influence on the spin-forbidden $^2E \rightarrow {}^4A_2$ transition of Cr^{3+} [25,42].

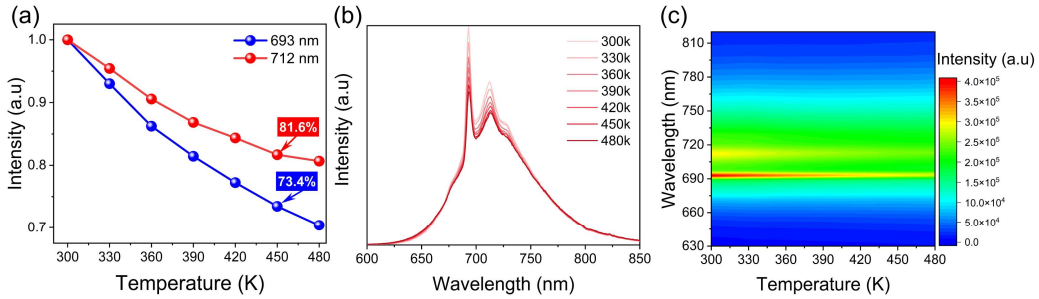

Figure 6. Emission intensities of 693 nm and 712 nm (**a**) and emission spectra; (**b**,**c**) of GAGG:0.1Cr^{3+}, 0.01Dy^{3+} dependent on temperatures.

3.5. LED Packages

In order to demonstrate the applicability of the synthetic GAGG:0.1Cr^{3+}, 0.01Dy^{3+} for indoor plant growth, LED devices were fabricated with the GAGG:0.1Cr^{3+}, 0.01Dy^{3+} phosphor and a 450 nm blue chip. Figure 7 shows the resultant CIE coordinates of this LED device, which were found at (0.6387, 0.2873). It appears as a milky white light in the LED device and provides a bright purplish-red emission driven by a current of 20 mA. It gives a strong red emission and yields a luminous efficacy of 27.8 lmW^{-1}. The results show that the new GAGG:0.1Cr^{3+},0.01Dy^{3+} phosphor can be excited by 450 nm of blue light and its red emission has a good overlap with the red light absorption of chlorophyll [8], demonstrating its potential for plant growth lighting and white LED lighting.

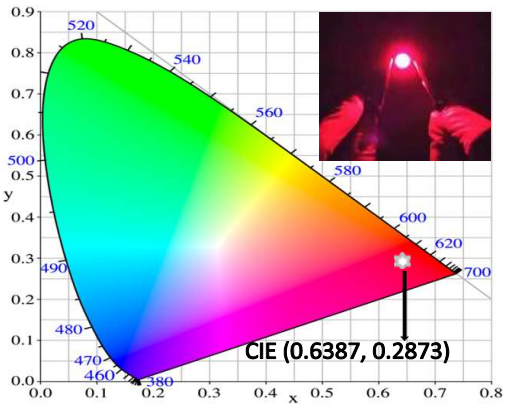

Figure 7. CIE chromaticity coordinates of the sample. The illustration shows the LED device in a 450nm chip package.

4. Conclusions

To sum up, Dy^{3+} and Cr^{3+} co-doped GAGG phosphors were successfully synthesized using a conventional high-temperature solid-state method. Dy^{3+} ions fit into Gd^{3+} sites and played the role of sensitizing the luminescence center for Cr^{3+}. The luminescence intensity in deep-red light (650–850 nm) was enhanced by Dy^{3+}/Cr^{3+} co-doping. The luminous intensity of optimized GAGG:Cr^{3+},0.01Dy^{3+} was 1.4 times that of the Cr^{3+} single-doped sample and its quantum efficiency was up to 86.65%. Many results point toward an energy transfer from Dy^{3+} to Cr^{3+} in GAGG:0.1Cr^{3+}, 0.01Dy^{3+} phosphors. Finally, LED devices made from GAGG:0.1Cr^{3+}, 0.01Dy^{3+} phosphors have good properties. This indicates potential applications of the phosphor in agriculture.

Author Contributions: Y.Z. contributed to study design, data collection, data analysis and writing; X.L. contributed to data collection, data interpretation and figures; D.H. contributed to literature search; Q.S. contributed to data interpretation; X.W. contributed to figures; F.W. contributed testing; K.W. contributed to testing; X.Z. contributed data collection; Z.S. contributed SEM testing; Y.L. contributed manuscript modification; K.C. contributed to study design, literature search, data interpretation. All authors have read and agreed to the published version of the manuscript.

Funding: This work is financially supported by the National Natural Science Foundation of Inner Mongolia (2019MS05030), the Science and Technology Plan of Inner Mongolia (2019GG263) and the Public Projects of the Zhejiang Province (LGG18E020007).

Data Availability Statement: Not applicable.

Conflicts of Interest: The authors declare no conflict of interest.

References

1. Yeh, N.; Chung, J.P. High-brightness LEDs—Energy efficient lighting sources and their potential in indoor plant cultivation. *Renew. Sustain. Energy Rev.* **2016**, *13*, 2175–2180. [CrossRef]
2. Qiu, Z.; Luo, T.; Zhang, J.; Zhou, W.; Yu, L.; Lian, S. A green approach to green-conversion material and green-agriculture: Alkaline-earth metal sulfide phosphors. *J. Mater. Chem. C.* **2015**, *3*, 9631–9636. [CrossRef]
3. Massa, G.D.; Kim, H.H.; Wheeler, R.M.; Mitchell, C.A. Plant productivity in response to LED lighting. *HortScience* **2018**, *43*, 1951–1956. [CrossRef]
4. Wu, T.; Lin, Y.; Zheng, L.; Guo, Z.; Xu, J.; Liang, S.; Chen, Z. Analyses of multi-color plant-growth light sources in achieving maximum photosynthesis efficiencies with enhanced color qualities. *Opt. Express* **2018**, *26*, 4135–4147. [CrossRef] [PubMed]
5. Yuan, W.; Pang, R.; Wang, S.; Tan, T.; Li, C.; Wang, C.; Zhang, H. Enhanced blue-light excited cyan-emitting persistent luminescence of $BaLu_2Al_2Ga_2SiO_{12}$:Ce^{3+}, Bi^{3+} phosphors for AC-LEDs via defect modulation. *Light Sci. Appl.* **2022**, *11*, 184. [CrossRef]
6. Yao, Q.; Hu, P.; Sun, P.; Liu, M.; Liu, R.; Chao, K.; Jiang, H. YAG:Ce^{3+} transparent ceramic phosphors brighten the next-generation laser-driven lighting. *Adv. Mater.* **2020**, *32*, 1907888. [CrossRef] [PubMed]
7. Jia, Z.; Yuan, C.; Liu, Y.; Wang, X.J.; Sun, P.; Wang, L.; Jiang, J. Strategies to approach high performance in Cr^{3+}-doped phosphors for high-power NIR-LED light sources. *Light Sci. Appl.* **2020**, *9*, 86. [CrossRef]
8. Olle, M.; Viršile, A. The effects of light-emitting diode lighting on greenhouse plant growth and quality. *Agric. Food Sci.* **2013**, *22*, 223–234. [CrossRef]
9. Dramićanin, M.D.; Marciniak, Ł.; Kuzman, S.; Piotrowski, W.; Ristić, Z.; Periša, J.; Ma, C.G. Mn^{5+}-activated $Ca_6Ba(PO_4)_4O$ near-infrared phosphor and its application in luminescence thermometry. *Light Sci. Appl.* **2020**, *11*, 1–13. [CrossRef]
10. Dang, P.; Li, G.; Yun, X.; Zhang, Q.; Liu, D.; Lian, H.; Lin, J. Thermally stable and highly efficient red-emitting Eu^{3+}-doped $Cs_3GdGe_3O_9$ phosphors for WLEDs: Non-concentration quenching and negative thermal expansion. *Light Sci. Appl.* **2021**, *10*, 29. [CrossRef]
11. Lei, L.; Wang, Y.; Kuzmin, A.; Hua, Y.; Zhao, J.; Xu, S.; Prasad, P.N. Next generation lanthanide doped nanoscintillators and photon converters. *ELight* **2022**, *2*, 17. [CrossRef]
12. Sadraeian, M.; Zhang, L.; Aavani, F.; Biazar, E.; Jin, D. Viral inactivation by light. *Elight* **2022**, *2*, 1–18. [CrossRef] [PubMed]
13. Huang, G.; Liu, Y.; Wang, D.; Zhu, Y.; Wen, S.; Ruan, J.; Jin, D. Upconversion nanoparticles for super-resolution quantification of single small extracellular vesicles. *ELight* **2022**, *2*, 20. [CrossRef]
14. Hu, T.; Ning, L.; Gao, Y.; Qiao, J.; Song, E.; Chen, Z.; Zhang, Q. Glass crystallization making red phosphor for high-power warm white lighting. *Light Sci. Appl.* **2021**, *10*, 56. [CrossRef] [PubMed]
15. Uheda, K.; Hirosaki, N.; Yamamoto, Y.; Naito, A.; Nakajima, T.; Yamamoto, H. Luminescence properties of a red phosphor $CaAlSiN_3$:Eu^{2+}, for white light-emitting diodes. *Electrochem. Solid State Lett.* **2006**, *9*, H22. [CrossRef]
16. Zhu, H.; Lin, C.C.; Luo, W.; Shu, S.; Liu, Z.; Liu, Y.; Chen, X. Highly efficient non-rare-earth red emitting phosphor for warm white light-emitting diodes. *Nat. Commun.* **2014**, *5*, 4312. [CrossRef]

17. Ueda, J.; Leaño, J.L.; Richard, C.; Asami, K.; Tanabe, S.; Liu, R.S. Broadband near-infrared persistent luminescence of Ba[$Mg_2Al_2N_4$] with Eu^{2+} and Tm^{3+} after red light charging. *J. Mater. Chem. C.* **2019**, *7*, 1705–1712. [CrossRef]
18. Menon, S.G.; Hebbar, D.N.; Kulkarni, S.D.; Choudhari, K.S.; Santhosh, C. Facile synthesis and luminescence studies of nanocrystalline red emitting Cr:$ZnAl_2O_4$ phosphor. *Mater. Res. Bull.* **2017**, *86*, 63–71. [CrossRef]
19. Fang, M.H.; Huang, P.Y.; Bao, Z.; Majewska, N.; Lesniewski, T.; Mahlik, S.; Liu, R.S. Penetrating biological tissue using light-emitting diodes with a highly efficient near-infrared $ScBO_3$:Cr^{3+} phosphor. *Chem. Mater.* **2020**, *32*, 2166–2171. [CrossRef]
20. Zeng, H.; Zhou, T.; Wang, L.; Xie, R.J. Two-site occupation for exploring ultra-broadband near-infrared phosphor-double-perovskite La_2MgZrO_6:Cr^{3+}. *Chem. Mater.* **2019**, *31*, 5245–5253. [CrossRef]
21. Rajendran, V.; Lesniewski, T.; Mahlik, S.; Grinberg, M.; Leniec, G.; Kaczmarek, S.M.; Liu, R.S. Ultra-broadband phosphors converted near-infrared light emitting diode with efficient radiant power for spectroscopy applications. *ACS Photon.* **2019**, *6*, 3215–3224. [CrossRef]
22. Feng, X.; Lin, L.; Duan, R.; Qiu, J.; Zhou, S. Transition metal ion activated near-infrared luminescent materials. *Prog. Mater. Sci.* **2022**, *129*, 100973. [CrossRef]
23. Liu, S.; Sun, P.; Liu, Y.; Zhou, T.; Li, S.; Xie, R.J.; Jiang, H. Warm white light with a high color-rendering index from a single $Gd_3Al_4GaO_{12}$:Ce^{3+} transparent ceramic for high-power LEDs and LDs. *ACS Appl. Mater. Interfaces* **2018**, *11*, 2130–2139. [CrossRef] [PubMed]
24. Elzbieciak, K.; Bednarkiewicz, A.; Marciniak, L. Temperature sensitivity modulation through crystal field engineering in Ga^{3+} co-doped $Gd_3Al_{5-x}Ga_xO_{12}$:Cr^{3+}, Nd^{3+} nanothermometers. *Sens. Actuators B Chem.* **2018**, *269*, 96–102. [CrossRef]
25. Zhang, L.; Zhang, S.; Hao, Z.; Zhang, X.; Pan, G.H.; Luo, Y.; Zhang, J. A high efficiency broad-band near-infrared $Ca_2LuZr_2Al_3O_{12}$:Cr^{3+} garnet phosphor for blue LED chips. *J. Mater. Chem. C.* **2018**, *6*, 4967–4976. [CrossRef]
26. Yao, L.; Shao, Q.; Xu, X.; Dong, Y.; Liang, C.; He, J.; Jiang, J. Broadband emission of single-phase $Ca_3Sc_2Si_3O_{12}$:Cr^{3+}/Ln^{3+} (Ln = Nd, Yb, Ce) phosphors for novel solid-state light sources with visible to near-infrared light output. *Ceram. Int.* **2019**, *45*, 14249–14255. [CrossRef]
27. Wu, J.; Zhuang, W.; Liu, R.; Liu, Y.; Gao, T.; Yan, C.; Chen, X. Broadband near-infrared luminescence and energy transfer of Cr^{3+}, Ce^{3+} co-doped $Ca_2LuHf_2Al_3O_{12}$ phosphors. *J. Rare Earths* **2021**, *39*, 269–276. [CrossRef]
28. Bilir, G.; Ozen, G.; Bettinelli, M.; Piccinelli, F.; Cesaria, M.; Di Bartolo, B. Broadband Visible Light Emission From Nominally Undoped and Cr^{3+} Doped Garnet Nanopowders. *IEEE Photon. J.* **2014**, *6*, 1–11. [CrossRef]
29. Rajendran, V.; Fang, H.M.; Huang, W.T.; Majewska, N.; Lesniewski, T.; Mahlik, S.; Liu, R.S. Chromium ion pair luminescence: A strategy in broadband near-infrared light-emitting diode design. *J. Am. Chem. Soc.* **2021**, *143*, 19058–19066. [CrossRef]
30. Shannon, R.D. Revised effective ionic radii and systematic studies of interatomic distances in halides and chalcogenides, Acta crystallographica section A: Crystal physics, diffraction. *Theor. Gen. Crystallogr.* **1976**, *32*, 751–767. [CrossRef]
31. Basavaraju, N.; Priolkar, K.R.; Gourier, D.; Bessière, A.; Viana, B. Order and disorder around Cr^{3+} in chromium doped persistent luminescent AB_2O_4 spinels. *Phys. Chem. Chem. Phys.* **2015**, *17*, 10993–10999. [CrossRef] [PubMed]
32. Guzmán-Rocha, M.; Oliva, J.; Diaz-Torres, L.A.; Montes, E. Effect of the reducing atmospheres on the photoluminescent and phosphorescent properties of $Sr_4Al_{14}O_{25}$:Eu^{2+}, Dy^{3+}, Cr^{3+} phosphors. *J. Sol Gel Sci. Technol.* **2020**, *95*, 423–431. [CrossRef]
33. Sharma, S.K.; Gourier, D.; Viana, B.; Maldiney, T.; Teston, E.; Scherman, D.; Richard, C. Persistent luminescence of AB_2O_4:Cr^{3+} (A = Zn, Mg, B = Ga, Al) spinels: New biomarkers for in vivo imaging. *Opt. Mater.* **2014**, *36*, 1901–1906. [CrossRef]
34. Yin, C.; Wang, R.; Jiang, P.; Cong, R.; Yang, T. Dy^{3+} and Tm^{3+} doped $YGa_3(BO_3)_4$ for near ultraviolet excited white phosphors. *J. Solid State Chem.* **2019**, *269*, 30–35. [CrossRef]
35. Devakumar, B.; Guo, H.; Zeng, Y.J.; Huang, X. A single-phased warm-white-emitting $K_3Y(PO_4)_2$:Dy^{3+}, Sm^{3+} phosphor with tuneable photoluminescence for near-UV-excited white LEDs. *Dye. Pigment.* **2018**, *157*, 72–79. [CrossRef]
36. Xu, Q.; Sun, J.; Cui, D.; Di, Q.; Zeng, J. Synthesis and luminescence properties of novel $Sr_3Gd(PO_4)_3$:Dy^{3+} phosphor. *J. Lumin.* **2015**, *158*, 301–305. [CrossRef]
37. Zhao, L.; Meng, D.; Li, Y.; Zhang, Y.; Wang, H. Tunable emitting phosphors $K_3Gd(PO_4)_2$:Tm^{3+}-Dy^{3+} for light-emitting diodes and field emission displays. *J. Alloys Compd.* **2017**, *728*, 564–570. [CrossRef]
38. Bai, Q.; Zhao, S.; Xu, Z.; Li, P. Tunable luminescence in co-doped $Zn_3Al_2Ge_2O_{10}$:Cr^{3+} by controlling crystal field splitting and nephelauxetic effect. *J. Rare Earths* **2020**, *38*, 1265–1272. [CrossRef]
39. Du, P.; Yu, J.S. Self-activated multicolor emissions in $Ca_2NaZn_2(VO_4)_3$:Eu^{3+} phosphors for simultaneous warm white light-emitting diodes and safety sign. *Dye Pigment.* **2017**, *147*, 16–23. [CrossRef]
40. Du, P.; Yu, J.S. Synthesis and luminescent properties of Eu^{3+}-activated $Na_{0.5}Gd_{0.5}MoO_4$: A strong red-emitting phosphor for LED and FED applications. *J. Lumin.* **2016**, *179*, 451–456. [CrossRef]
41. Zhou, Z.; Li, Y.; Xia, M.; Zhong, Y.; Zhou, N.; Hintzen, H.B. Improved luminescence and energy-transfer properties of $Ca_{14}Al_{10}Zn_6O_{35}$:Ti^{4+}, Mn^{4+} deep-red-emitting phosphors with high brightness for light-emitting diode (LED) plant-growth lighting. *Dalton Trans.* **2018**, *47*, 13713–13721. [CrossRef] [PubMed]
42. Ueda, J.; Tanabe, S. Visible to near infrared conversion in Ce^{3+}-Yb^{3+} co-doped YAG ceramics. *J. Appl. Phys.* **2009**, *106*, 043101. [CrossRef]